Two-Terminal and Multi-Terminal Designs for Next-Generation Quantized Hall Resistance Standards: Contact Material and Geometry

Two-terminal and multi-terminal designs for next generation quantized Hall resistance standards: contact material and geometry

Mattias Kruskopf*, Albert F. Rigosi, Alireza R. Panna, Dinesh K. Patel, Hanbyul Jin, Martina Marzano, Michael Berilla, David B. Newell, and Randolph E. Elmquist, *Senior Member, IEEE*

***Abstract*—Here we show that precision quantum Hall resistance measurements using two terminals may be as precise as four-terminal measurements when applying superconducting split contacts. The described sample designs minimize undesired resistances at contacts and interconnections such that the size and complexity of next generation quantized Hall resistance devices can be significantly improved.**

***Index Terms*— quantum Hall effect, quantized Hall resistance standards, epitaxial graphene, superconducting contacts, multiple-series contacts**

I. Introduction

Quantum effects in epitaxial graphene devices allow for robust quantum Hall effect (QHE) resistance plateaus at $R_H = R_K/2 = h/2e^2$, where R_H is the Hall resistance and R_K is the von Klitzing constant [1]–[3]. By using series and parallel connections as building blocks, one can construct quantum Hall array resistance standards (QHARS) that provide multiple quantized resistance values [4]–[9]. However, resistance networks based on multiple QHR devices often suffer from accumulated resistances at contacts and interconnections. In this work we show that quantized resistances normally measured at four terminals for high precision can also be measured at two terminals by eliminating undesired resistances when applying superconducting split contacts. While multi-series (MS) interconnections of QHE devices have been extensively studied and applied for the construction of QHARS, we show that the principle can also be applied to significantly improve the performance of contacts of single QHR elements. Together with using superconducting materials these improvements open new routes in the design of next generation resistance standards.

II. Device Preparation and Characterization

The device fabrication process presented in Figure 1(a) is based on the technique of protecting the epitaxial graphene (EG) from lithographic residues with a thin Pd/Au layer to allow for contaminant-free graphene/metal contacts [10], [11]. The covered EG is then structured into the Hall bar geometry using a thicker Au metal masking layer and Ar plasma etching. The ≈ 320 nm thick superconducting NbTiN layer for the contacts and contact pads is sputtered onto a ≈ 7.5 nm thin Ti adhesion layer and is then covered by ≈ 30 nm Pt to prevent surface oxidation. In the last step, photolithography is applied to open a window to the Pd/Au covered EG which is then wet-etched using diluted aqua regia. The wet-etching procedure removes the Pd/Au in the defined areas without harming the EG. The finished devices are functionalized with chromium tricarbonyl [$Cr(CO)_3$], which provides tunable and uniform doping without the need for large-scale electrostatic gates [12].

To assess the superconducting behavior of the contacts, the resistance of a finished device was monitored as a function of temperature with a lock-in amplifier system. As shown in Figure 1(b), two points shorted by a NbTiN element exhibit a discontinuous reduction in the four-wire resistance after falling below the critical temperature (T_c) of about 12.5 K at zero field. Using a nanovoltmeter and a current-reversal measurement technique to eliminate thermal voltages, the resistance at 1.6 K was determined to be zero (-0.31 μΩ ± 3.63 μΩ) within the measurement uncertainty. At B = 9 T the critical temperature was reduced by about 2 K, and is still far above the typical measurement temperature of ≤ 4.2 K.

Figure 1(c) shows a confocal laser scanning microscope (CLSM) image of a graphene device source/drain (S/D) region with superconducting split contacts with six branches. Labels indicate the high and low equipotential edges, separated by hot spots that appear in the quantum Hall regime and mark the points where dissipation occurs [13], [14]. Depending on the direction of the applied magnetic field, the hot-spots occur in different corners of the device. For interconnected S/D contact points separated by more than an inelastic scattering length most of the current enters via the very first branch (C_1), closest to the corner [15]. Thus, for multiple-series quantum Hall effect devices the current in each of the following branches denoted by C_2, …, C_n of a split contact is progressively lower by factors of $\varepsilon/2 = (R_{branch}/R_H)/2$ [4]. In the case of three or more distinct branches with individual contact resistances on the order of R_{branch} = 1 Ω to 10 Ω, the current in the last branch (C_n) becomes negligible and thus the overall contact resistance is negligibly

Manuscript submitted March 9, 2019. For a subset of the author list, this work was prepared as part of their official duties for the U. S. Government. *Asterisk indicates corresponding author.*

M. Kruskopf, and H. Jin are Postdoctoral Associates at the Joint Quantum Institute, University of Maryland, Department of Physics College Park, MD 20742, while working at the National Institute of Standards and Technology (NIST) in Gaithersburg. (emails: mattias.kruskopf@nist.gov and hanbyul.jin@nist.gov).

Martina Marzano is with the Politecnico di Torino, Istituto Nazionale di Ricerca Metrologica, Turin, Italy (email: m.marzano@inrim.it).

D. Patel is with the Graduate Institute of Applied Physics, National Taiwan University, Taipei 10617, Taiwan (email: dkpjnp@gmail.com).

A. F. Rigosi, A. R. Panna, M. Berilla, D. B. Newell, and R. E. Elmquist are employees of the National Institute of Standards and Technology, Gaithersburg, MD 20899, USA (e-mails: albert.rigosi@nist.gov, alireza.panna@nist.gov, michael.berilla@nist.gov, david.newell@nist.gov and randolph.elmquist@nist.gov)

small.

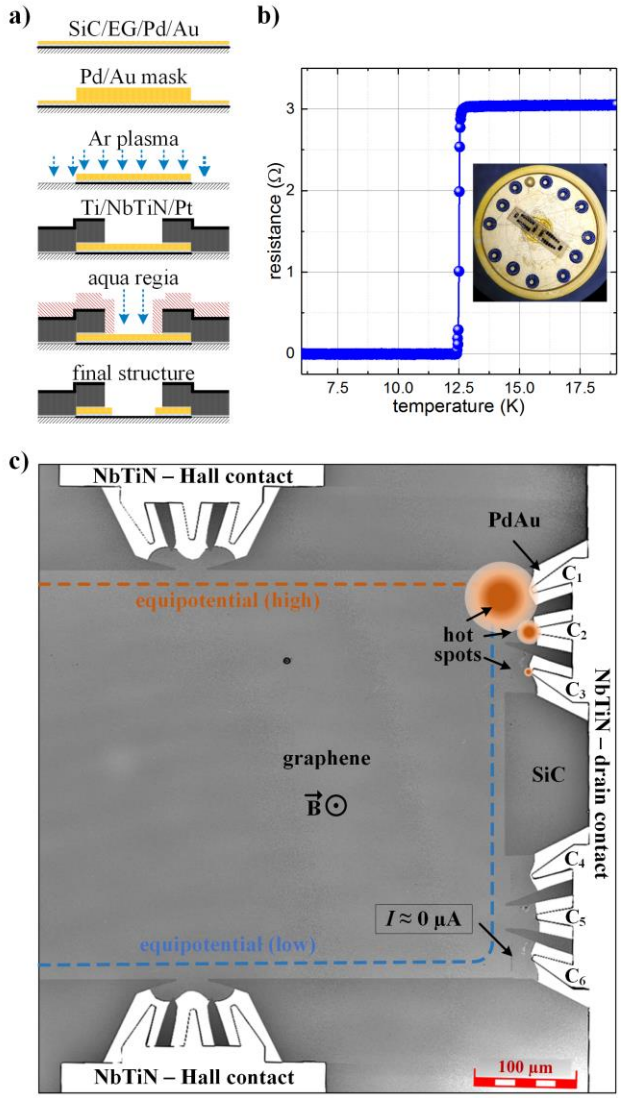

Figure 1. (a) The photolithography process for graphene device fabrication using superconducting NbTiN contacts is divided into six steps (from the top to the bottom) (b) Resistance measurements of the superconducting NbTiN contacts show vanishing resistance below the critical transition temperature T_c ≈ 12.5 K. The inset represents the top-view onto the sample with two devices mounted onto a TO-8 header. (c) The confocal laser scanning microscope image of a graphene Hall device shows the structured graphene (light grey structure) as well as the drain contact (right) and two Hall contacts (top and bottom). By splitting each contact into multiple individual branches, the resulting contact resistance becomes negligible in the quantum Hall regime. The drawn hot spots at the contacts indicate that most of the current enters the first branch (C_1) of the contact while the current is reduced by $\varepsilon/2$. The current in the last branch I_{C6} ≈ 0 µA describes equilibrium between the electric potential of the contacts and the QHE edge channels as well as an approximately zero contact S/D resistance.

III. Results and Discussion

To test the performance of the split contacts, three different processes/designs for making device contacts were tested. The left side of Figure 2(a) shows that device 1 (NbTiN) and device 2 (Au) use the same design but a different main contact material component. The corresponding measurement for device 1 on the right of Figure 2(a) shows the typical magnetic field dependence in the standard four-terminal resistance measurement configuration of epitaxial graphene-based QHE devices. At the measurement temperature of 1.6 K the charge carrier density and mobility were $n = 1.33 \times 10^{11}$ cm^{-2} and μ = 15040 cm^2/Vs, respectively.

Device 3, as shown on the left in Figure 2(b), has multiple-series (MS) connections at the high and low potential sides of the Hall bar. This design provides an optimum measurement configuration for one magnetic field direction, where hot spots are shown in blue, because the influence of remnant longitudinal resistivity is minimized as with an ideal four-terminal configuration. The resistance across the S/D contacts in the two-terminal/MS configuration shown on the right side of Figure 2(b) is symmetric in the two field directions, with an extended resistance plateau starting around $B = \pm 5$ T. The high dependence of the longitudinal resistance on the B-field direction shown in Figure 2(b) is due to the asymmetric current path for positive and negative field directions at low fields. The changing positions of the hot spots when going from B = +9 T to B = -9 T is indicated by the blue and red spots, respectively.

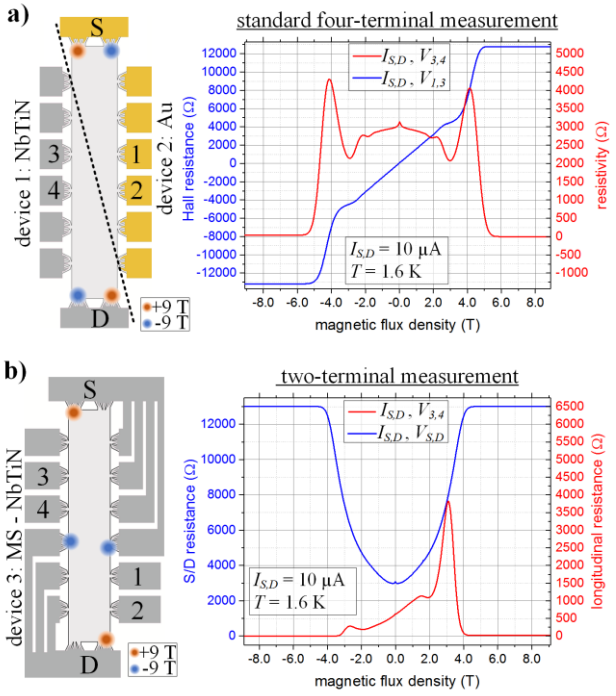

Figure 2 (a) Device 1 (NbTiN contacts) and device 2 (Au contacts) represent typical devices for standard four-terminal/four-contact QHR measurements. The corresponding magnetic field sweep of device 1 shows the behavior of the Hall resistance with a linear slope at low fields (2 T > B > -2 T) and QHR plateaus of converse sign at high fields above ± 5.5 T. The hot spots for the opposite magnetic field direction are shown in red. The longitudinal resistivity is highly symmetric in both field directions. (b) Device 3 (MS - NbTiN) uses a multi-series (MS) connection for two-terminal measurements to eliminate contributions of the longitudinal resistance when operating at + 9T. The magnetic field dependence of the resistance in the two-terminal configuration across the source/drain (S/D) contacts shows a symmetrical, non-linear behavior at low fields up to $B = \pm 4.5$ T and extended resistance plateaus at high fields of $|B| \geq 5$ T). The longitudinal resistance shows an asymmetrical behavior depending on the direction of the magnetic field due to significant changes in the current path. The expected positions of the hot spots in the quantum Hall regime are indicated by the red and blue marked locations for positive and negative magnetic flux densities. The numbers and labels of the contacts describe the ones that were used for the measurements as given in the legends.

The precision measurements in Figure 3(a) were performed using a direct current comparator (DCC) resistance bridge [16] for device 1 (NbTiN) and a binary cryogenic current comparator (BCCC) bridge [17] for device 2 (Au) and device 3 (MS - NbTiN). We determined the resistance value in the two-terminal configuration using four wires (blue triangles) and the standard four-terminal configuration (red stars). The pin configuration can be understood from the numbers and labels given in the legend of the measurements and the drawings of the devices in Figure 2. The deviation from the nominal QHR value is calculated from $\delta = (R - R_K/2)/R$, where R is the measured Hall resistance. In the four-terminal measurement configuration, the deviation from nominal was -1.4 nΩ/Ω ±21 nΩ/Ω for device 1 and 5.3 nΩ/Ω ±9.8 nΩ/Ω for device 2. In the two-terminal configuration, the deviation was 19 nΩ/Ω ±17 nΩ/Ω, 620 nΩ/Ω ±7.9 nΩ/Ω and 12 nΩ/Ω ±3.5 nΩ/Ω for device 1, device 2 and device 3, respectively. The uncertainties show the type A uncertainties ($k = 1$). Under the assumption of perfect quantization, implying a negligible contribution of the longitudinal resistance in the two-terminal resistance measurement, one can estimate the S/D contact resistance R_{cont} from the difference $\Delta = R - (R_K/2)$ where $R_{cont} = \Delta/2$ [18]. The resulting contact resistances are 124 μΩ ±110 μΩ, 4029 μΩ ±51 μΩ and 77 μΩ ±22 μΩ for device 1, device 2 and device 3, respectively. Under the more realistic assumption of a non-zero longitudinal resistivity of about 10 μΩ/square the contact resistances of device 1 and device 2 are even lower, considering the 5.5 squares (each 400 μm × 400 μm) describing the Hall bar.

Figure 3(b) shows longitudinal resistance data from the low equipotential side of the three devices taken using an analog nanovoltmeter, with direct current (dc) reversal to eliminate thermal voltages. The red stars show standard longitudinal resistance measurements in the four-terminal configuration by measuring the voltage between two neighboring Hall contacts 3 and 4. The blue triangles describe the resistance across the Hall contact 3 and the drain contact in a three-terminal configuration. Any significant difference in the two is expected to be due to the voltage drop at the drain contact. The results of the devices 1 and 3 using superconducting split contacts are consistent with the measurements in Figure 3(a) and support the understanding that the contact resistance and the longitudinal resistance are indeed both close to zero within the measurement uncertainty. A clear deviation from zero 580 μΩ ±260 μΩ was observed when measuring across the Au Hall and drain contact of device 2. The slightly lower value compared to the one determined from the measurement in Figure 3(a) suggests that sample inhomogeneities have led to higher longitudinal resistances in some parts of this device. Since Ti/Au contacts of graphene quantum Hall devices reported in the literature have typically yielded contact resistances of 1 Ω or higher [19], this work reports on the order of 10^4 times lower resistances compared to most previously reported values.

Figure 3(c) shows further investigations of the longitudinal resistance and contact resistance behavior using three terminals at high currents of device 1 (NbTiN, blue data points) and device 2 (Au, red data points). The data shows a strong increase in the resistance when measuring between the Hall contact 3 and the drain contact in the case of device 2. In the case of device 1, the resistance was surprisingly unaffected with a near-zero value of 302 μΩ ± 334 μΩ when applying the highest current of 771 μA.

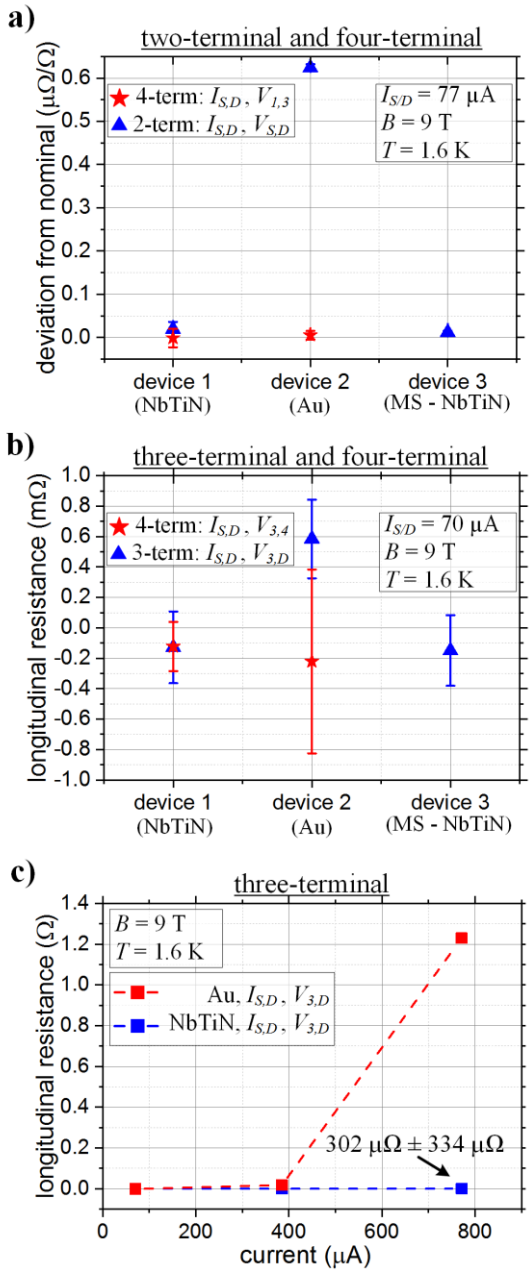

Figure 3. (a) Precision QHR measurements using CCC (cryogenic current comparator) and DCC (direct current comparator) measurement systems show the deviation of the measured resistance from the nominal value of $R_K/2 = h/2e^2$ ≈ 12906.4 Ω. Device 1 (NbTiN) and device 2 (Au) were measured in the standard four-terminal (4-term, red stars) and two-terminal (2-term, blue triangles) measurement configuration while device 3 (MS NbTiN) was measured in the two-terminal configuration only. The labeling of the pins used for the measurements given in the legend corresponds to the labels given in Figure 2. In the two-terminal configuration, the deviation from nominal is on the order of 10 nΩ/Ω when using NbTiN contacts and approximately 600 nΩ/Ω in the case of Au contacts. In the standard four-terminal configuration the deviation from nominal is 0 nΩ/Ω within the measurement uncertainty. The error bars indicate the type A uncertainty ($k = 1$) of the measurements. (b) Longitudinal measurements at the low potential side of the Hall bar were performed applying dc current reversal and using a nanovoltmeter. The

longitudinal resistances were determined by measuring the voltage drop between neighboring Hall contacts using four terminals (4-term, red stars) as well as between a Hall contact and the drain contact using three terminals (3-term, blue triangles). The vanishing three-terminal longitudinal resistance across the drain contact indicates exceptionally small effective contact resistances in the case of device 1 (NbTiN) and device 3 (MS-NbTiN). The error bars indicate the standard deviation of the measurements. (c) In contrast to Au contacts (device 2, red square), three-terminal longitudinal resistance measurements between the Hall and drain contact show no significant current dependence at currents as high as 771 µA in the case of NbTiN contacts (device 1, blue square).

State-of-the-art series-connected QHR elements require complicated lithography steps to realize multi-layer interconnections and to ensure that the Hall contacts have no electrical contact to the S/D contacts while crossing the current path [6], [20]. This is to avoid picking up any Hall voltages occurring in the S/D metal contact pads as well as voltages due to the S/D current and ohmic resistance in the region of the current terminals. The realization of QHE devices with vanishing contact resistances and no additional dissipation at interconnections provided using superconducting materials, allows for significant simplifications in the design of future quantized resistance standards. In Figure 4 three miniaturized QHE elements are proposed that may be used in resistance metrology as individual devices or as the smallest cell for the construction of QHARS.

The element in Figure 4(a) is designed to provide a quantized resistance value that is free of longitudinal resistance contributions since the Hall voltage is defined in the center of the two sides. It is especially suitable for the construction of series-connected elements in arrays because of its optimized two-terminal design. It sacrifices the additional contact used to measure the value of the longitudinal resistance to minimize the size. Using a superconductor instead of normal metallic interconnections eliminates undesired contributions at these interconnections such that voltage and current terminals can be the same. Note that the superconductor must have a critical temperature and a critical field significantly above the measurement conditions to avoid the occurrence of non-zero Hall fluctuations [21], [22].

As demonstrated by the results of device 1 and device 2 in Figure 2, superconducting split contacts allow for precise measurements in the two-terminal and in the four-terminal definition. The design proposed in Figure 4(b) condenses the multi-terminal Hall bar design to the minimum number of contacts while maintaining access to both Hall and longitudinal measurements. Note that when performing longitudinal measurements between the low-potential Hall contact and drain, the result is always a sum of the contact resistance and the longitudinal resistance in the edge channels [18]. Figure 4(c) is the smallest possible QHARS element and may only be used in the two-terminal configuration, like the design in Figure 4(a). Even though longitudinal resistance in the 2D region may affect the value of the QHR in this design, the smaller square design reduces both the channel length and the resulting longitudinal resistance by a factor of two. For highly uniform epitaxial graphene, the introduced error is expected to be small enough to allow for measurements with a deviation from nominal on the order of 10 nΩ/Ω or less. The reduction in complexity and size would also help to minimize capacitive losses at alternating current, and might allow for ac-QHE measurements with improved precision compared to formerly used designs [23], [24].

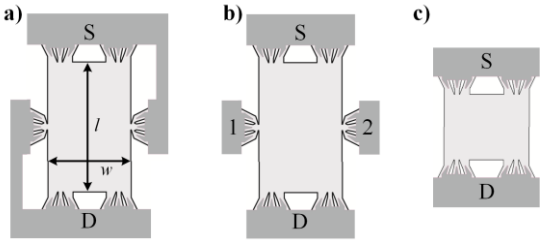

Figure 1 (a) This element combines the principle of superconducting split contacts and a double series connection. Since the Hall voltage is defined in the center of the device, no longitudinal resistance component is added to the measurement. When deployed in QHARS networks this element allows for miniaturized designs and simplified processing by eliminating the need of multilayer lithography processes. (b) Removing the series connection allows for two-terminal as well as standard four-terminal measurements. (c) Removing the Hall contacts results in the most compact and simplest design. Such elements with reduced complexity may be beneficial for ac-QHR measurements due to potentially reduced capacitive losses. An appropriate width to length ratio of the QHR channel for the designs given in (a), (b) and (c) is suggested to be w/l = ½, w/l = ½ and w/l = 1, respectively.

IV. Conclusion

While normally measured at four terminals for high precision, here we demonstrate that the quantized Hall resistance can be precisely measured at two terminals. Because the QHE itself selects preferred current terminals depending on the B-field direction, the split-contacts using six branches at the S/D terminals allow for voltage and resistance measurements that are unaltered by contact resistances. Additionally, the application of superconducting materials eliminates undesired ohmic resistances and Hall voltages in the terminals. These improvements enable new avenues of device design for future resistance standards using crossover-free series and parallel connected elements and will help to minimize capacitive losses at alternating currents for impedance standards. As shown in this work, the principle of combining superconductivity and optimized contact design has great potential to improve the performance of single QHR standards and QHARS devices.

Acknowledgment

The work of D.P. at NIST was made possible by arrangement with C.-T. Liang of National Taiwan University, and the work of M.M. at NIST was made possible by arrangement with M. Ortolano of Polytechnic University of Turin and L. Callegaro of the Istituto Nazionale di Ricerca Metrologica, Turin, Italy.

References

[1] K. V. Klitzing and G. Ebert, “Application of the Quantum Hall Effect in Metrology,” *Metrologia*, vol. 21, no. 1, pp. 11–18, Jan. 1985.

[2] K. S. Novoselov *et al.*, “Two-dimensional gas of massless Dirac fermions in graphene,” *Nature*, vol. 438, no. 7065, pp. 197–200,

2005.
[3] T. J. B. M. Janssen *et al.*, "Precision comparison of the quantum Hall effect in graphene and gallium arsenide," *Metrologia*, vol. 49, no. 3, pp. 294–306, 2012.
[4] F. Delahaye, "Series and parallel connection of multiterminal quantum Hall-effect devices," *J. Appl. Phys.*, vol. 73, no. 11, pp. 7914–7920, 1993.
[5] W. Poirier, A. Bounouh, F. Piquemal, and J. P. André, "A new generation of QHARS: Discussion about the technical criteria for quantization," *Metrologia*, vol. 41, no. 4, pp. 285–294, 2004.
[6] T. Oe, S. Gorwadkar, T. Itatani, and N.-H. Kaneko, "Development of 1 MΩ Quantum Hall Array Resistance Standards," *IEEE Trans. Instrum. Meas.*, vol. 66, no. 6, pp. 1475–1481, Jun. 2017.
[7] A. Lartsev, S. Lara-Avila, A. Danilov, S. Kubatkin, A. Tzalenchuk, and R. Yakimova, "A prototype of Rk /200 quantum Hall array resistance standard on epitaxial graphene," *J. Appl. Phys.*, vol. 118, no. 4, p. 044506, Jul. 2015.
[8] M. Ortolano, M. Abrate, and L. Callegaro, "On the synthesis of quantum Hall array resistance standards," *Metrologia*, vol. 52, no. 1, pp. 31–39, 2015.
[9] S. Novikov *et al.*, "Mini array of quantum Hall devices based on epitaxial graphene," *J. Appl. Phys.*, vol. 119, no. 17, p. 174504, May 2016.
[10] M. Kruskopf and R. E. Elmquist, "Epitaxial graphene for quantum resistance metrology," *Metrologia*, vol. 55, no. 4, pp. R27–R36, Aug. 2018.
[11] Y. Yang *et al.*, "Epitaxial graphene homogeneity and quantum Hall effect in millimeter-scale devices," *Carbon N. Y.*, vol. 115, pp. 229–236, May 2017.
[12] A. F. Rigosi *et al.*, "Gateless and reversible Carrier density tunability in epitaxial graphene devices functionalized with chromium tricarbonyl," *Carbon N. Y.*, vol. 142, pp. 468–474, Feb. 2019.
[13] J. Weis and K. von Klitzing, "Metrology and microscopic picture of the integer quantum Hall effect," *Philos. Trans. R. Soc. A Math. Phys. Eng. Sci.*, vol. 369, no. 1953, pp. 3954–3974, Oct. 2011.
[14] K. Ikushima, H. Sakuma, S. Komiyama, and K. Hirakawa, "Visualization of quantum Hall edge channels through imaging of terahertz emission," *Phys. Rev. B*, vol. 76, no. 16, p. 165323, Oct. 2007.
[15] M. Büttiker, "Absence of backscattering in the quantum Hall effect in multiprobe conductors," *Phys. Rev. B*, vol. 38, no. 14, pp. 9375–9389, Nov. 1988.
[16] M. P. MacMartin and N. L. Kusters, "A Direct-Current-Comparator Ratio Bridge for Four-Terminal Resistance Measurements," *IEEE Trans. Instrum. Meas.*, vol. 15, no. 4, pp. 212–220, 1966.
[17] M. Gotz and D. Drung, "Stability and Performance of the Binary Compensation Unit for Cryogenic Current Comparator Bridges," *IEEE Trans. Instrum. Meas.*, vol. 66, no. 6, pp. 1467–1474, Jun. 2017.
[18] G. L. J. A. Rikken *et al.*, "Two-terminal resistance of quantum Hall devices," *Phys. Rev. B*, vol. 37, no. 11, pp. 6181–6186, Apr. 1988.
[19] T. Yager *et al.*, "Low contact resistance in epitaxial graphene devices for quantum metrology," *AIP Adv.*, vol. 5, no. 8, p. 087134, Aug. 2015.
[20] J. Könemann, C. Leicht, F.-J. Ahlers, E. Pesel, K. Pierz, and H. W. Schumacher, "Investigation of Serial Quantum Hall arrays as a Quantum Resistance Standard," *J. Phys. Conf. Ser.*, vol. 334, no. 1, p. 012017, Dec. 2011.
[21] N. P. Breznay and A. Kapitulnik, "Observation of the ghost critical field for superconducting fluctuations in a disordered TaN thin film," *Phys. Rev. B*, vol. 88, no. 10, p. 104510, Sep. 2013.
[22] D. Destraz, K. Ilin, M. Siegel, A. Schilling, and J. Chang, "Superconducting fluctuations in a thin NbN film probed by the Hall effect," *Phys. Rev. B*, vol. 95, no. 22, pp. 1–6, 2017.
[23] M. E. Cage and A. Jeffery, "A problem in ac quantized Hall resistance measurements and a proposed solution," *J. Res. Natl. Inst. Stand. Technol.*, vol. 103, no. 6, p. 593, Nov. 1998.
[24] C.-C. Kalmbach *et al.*, "Towards a graphene-based quantum impedance standard," *Appl. Phys. Lett.*, vol. 105, no. 7, p. 073511, Aug. 2014.

Mattias Kruskopf was born in Hamburg, Germany, in 1984. He received the M.Sc. degree in electronics engineering, with the focus on metrology from the Bremen University of Applied Sciences, Bremen, Germany, in 2013. In 2017, he received his Ph.D. degree for his research on epitaxial graphene for quantum resistance metrology in the working group of Low-dimensional Electron Systems at the Physikalisch-Technische Bundesanstalt (PTB), Braunschweig, Germany.

In his current research at the National Institute of Standards and Technology (NIST), Gaithersburg, MD, as a Postdoctoral Associate he is focusing on scalability improvements and the adoption of graphene-based resistance standards.

Albert F. Rigosi (M'17) was born in New York, NY, USA in 1989. He received the B.A., M.A., M.Phil., and Ph.D. degrees in physics from Columbia University, New York, NY, in 2011, 2013, 2014, and 2016, respectively.

From 2008 to 2015, he was a Research Assistant with the Columbia Nano Initiative. From 2015 to 2016, he was a Joint Visiting Research Scholar with the Department of Applied Physics of Stanford University in Stanford, CA, and the PULSE Institute of SLAC National Accelerator Laboratory in Menlo Park, CA. Since 2016, he has been a Physicist at the National Institute of Standards and Technology in Gaithersburg, MD. His research interests include two-dimensional electron systems and applications of those systems' behaviors for electrical metrology.

Dr. Rigosi is a member of the American Physical Society and the Mellon-Mays Initiative of The Andrew W. Mellon Foundation. He was awarded associateships and fellowships from the National Research Council (USA), the Optical Society of America, the Ford Foundation, and the National Science Foundation (Graduate Research Fellowship Program).

Alireza Panna was born in Mumbai, India. He received the B.S. degree in Electrical Engineering from the University of Maryland, College Park, MD, USA, in 2013. From 2012 to 2013 he worked as a guest researcher for the National Institutes of Standards and Technology, Gaithersburg, MD, USA, where he was involved in magnet characterization for the NIST-4 watt balance. From 2013 to 2017 he was with the National Institute of Health, Bethesda, MD, USA, where he worked on controls and characterization of various x-ray imaging modalities. He is currently with the National Institute of Standards and Technology where he is involved in the Metrology of the Ohm and the Quantum Conductance Projects.

Hanbyul Jin received the M.S./PhD degrees in electrical engineering studying wide bandgap semiconductors and graphene at Ulsan National Institute of Science and Technology (UNIST), Ulsan, Korea. Previous to that, he was a Visiting Researcher at Texas State University, San Marcos, TX working in Molecular beam epitaxy and compound semiconductors.

Since 2018, he has served as a Postdoctoral Associate at the Joint Quantum Institute, University of Maryland, Department of Physics while working at the National Institute of Standards and Technology (NIST) in Gaithersburg, MD.

Dinesh Kumar Patel was born in Uttar-Pradesh, India. He received the B. Sc and M. Sc degree in physics from Purvanchal University Jaunpur, Uttar-Pradesh, India as well as M. Tech degree in materials science at the Indian Institute of Technology Kanpur (IITK). From 2014 to 2015 he worked as a research assistant in Department of Physics, Indian Institute of Technology Delhi (IITD), New-Delhi, India. In 2015 he started his Ph.D. study at the Graduate Institute of Physics, National Taiwan University, Taiwan. From August 2018 till January 2020 he worked as a guest researcher at the National Institute of Standards and Technology (NIST), Gaithersburg, USA.

His current research field is about epitaxial graphene p-n-junctions for quantum Hall resistance standards.

Martina Marzano was born in Turin, Italy, in 1989. She received the master's degree in physics from the Università di Torino, Turin, Italy, in 2016. She is currently pursuing the PhD degree with the Politecnico di Torino, Turin, in collaboration with the Istituto Nazionale di Ricerca Metrologica, Turin. From 2018 to 2019, she was a guest researcher for six months at the National Institute of Standards and Technology in Gaithersburg, MD, US.

Her current research is focused on the development and modelling of devices and measurement methods for resistance and impedance metrology.

Michael Berilla received the B.S. degree in electrical engineering from Lehigh University, Bethlehem, PA, USA, in 2009, and the M.S. degree in electronics engineering from Drexel University, Philadelphia, PA, USA, in 2013.

From 2009 to 2015, he joined Lockheed Martin, Bethesda, MD, USA, where he became a Senior Electrical Engineer. Since 2015, he has been an Electronics Engineer with the Quantum Measurement Division, National Institute of Standards and Technology, Gaithersburg, MD, USA, where he is involved in precision measurement systems.

David B. Newell received his B.S. in physics and B.A. in mathematics from the University of Washington, Seattle and his Ph. D. in physics from the University of Colorado.

He was awarded a NRC postdoctoral fellowship to work on the Watt Balance Project at the National Institute of Standards and Technology (NIST) in Gaithersburg, MD, and became a full-time staff member in 1996. He has worked on measurements for realizing micro- and nano-scale forces traceable to the SI, was leader the Fundamental Electrical Measurements (FEM) group from 2004 to 2010, helped establish the use of graphene in quantum electrical standards, worked with a NIST team to construct a new watt balance to realize the kilogram from a fixed value of the Planck constant, and, as chair of the CODATA Task Group on Fundamental Constants, provided the exact values of the fundamental constants to be used in the new SI.

He has presently again accepted responsibility as leader of the FEM group. He is a member of the Philosophical Society of Washington, chair for the CODATA Task Group on Fundamental constants, and Fellow of the American Physical Society.

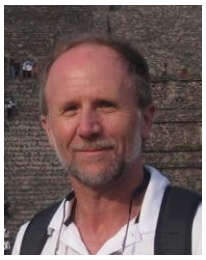

Randolph E. Elmquist (M'90–SM'98) received the Ph.D. degree in physics from the University of Virginia, Charlottesville, VA, in 1986. He leads the Quantum Conductance project at the NIST. Working for the past 32 years in the field of electrical and quantum metrology, he has contributed to the experimental design and measurement of the electronic Kilogram and calculable impedance standards for the determination of the von Klitzing constant and alpha, the unitless fine structure constant. He leads the development of cryogenic current comparator systems, the quantum Hall effect, and graphene electronic devices for metrology.

Dr. Elmquist is a member of the American Physical Society.